Investigation of morphometric parameters for granulocytes and lymphocytes as applied to a solution of direct and inverse light-scattering problems

Gennady I. Ruban
National Academy of Sciences of Belarus
Stepanov Institute of Physics
Nezavisimosti Avenue 68
Minsk 220072, Belarus
E-mail: ruban@dragon.bas-net.by

Svetlana M. Kosmacheva
Natalia V. Goncharova
Ministry of Health of Belarus
Centre of Hematology and Transfusiology
Dolginovsky Avenue 160
Minsk 223059, Belarus

Dirk Van Bockstaele
Antwerpen University and Hospital
Wilrijkstraat 10
Edegem B-2650, Belgium

Valery A. Loiko
National Academy of Sciences of Belarus
Stepanov Institute of Physics
Nezavisimosti Avenue 68
Minsk 220072, Belarus

Abstract. Quantitative data on cell structure, shape, and size distribution are obtained by optical measurement of normal peripheral blood granulocytes and lymphocytes in a cell suspension. The cell nuclei are measured *in situ*. The distribution laws of the cell and nuclei sizes are estimated. The data gained are synthesized to construct morphometric models of a segmented neutrophilic granulocyte and a lymphocyte. Models of interrelation between the cell and nucleus metric characteristics for granulocyte and lymphocyte are obtained. The discovered interrelation decreases the amount of cell-nucleus size combinations that have to be considered under simulation of cell scattering patterns. It allows faster analysis of light scattering to discriminate cells in a real-time scale. Our morphometric data meet the requirements of scanning flow cytometry dealing with the high rate analysis of cells in suspension. Our findings can be used as input parameters for the solution of the direct and inverse light-scattering problems in scanning flow cytometry, dispensing with a costly and time-consuming immunophenotyping of the cells, as well as in turbidimetry and nephelometry. The cell models developed can ensure better interpretations of scattering patterns for an improvement of discriminating capabilities of immunophenotyping-free scanning flow cytometry.
[DOI: 10.1117/1.2753466]

Keywords: cell model; light scattering; size distribution.

Paper 06167RR received Jun. 30, 2006; revised manuscript received Mar. 7, 2007; accepted for publication Apr. 19, 2007; published online Jul. 5, 2007.

1 Introduction

Particulate matter is widely investigated by various methods of remote optical probing. Among these methods are, for example, turbidimetry, nephelometry, and flow cytometry. Turbidimetry and nephelometry are based on light scattering by ensembles of particles, while flow cytometry[1–3] is based on single-particle analysis. Flow cytometry has been quickly developed within the last three decades. It is generally applied for characterization of single cells from light scattering and fluorescence. This technique deals with high rate analysis of particles (up to 5000 particles per second) and has numerous applications.[1,2,4] It is widely applied for the identification of white blood cells (leukocytes) by combining light scattering and immunophenotyping.[1] The latter is a time-consuming process. It utilizes expensive fluorescently labeled monoclonal antibodies. The possibility of cell injury should not be ruled out during immunophenotyping. Therefore, for the last few years a growing interest in the retrieval of morphological parameters of biological cells based mainly on scattering data has been observed. In conventional flow cytometry, scattered light is measured in two directions: forward and sideways. It is possible to extract more information about cell characteristics by measuring angular distributions of scattered light intensity or polarization, which are highly sensitive to cell morphology.

In some advanced experimental cytometric equipment apparatus, named scanning flow cytometers, the role of scattered radiation is extended. They measure angular dependences of intensity and polarization of scattered light ("fingerprints") over a wide interval of scattering angles.[5–8] The flow cytometric light-scattering patterns give new opportunities for retrieval of morphological parameters of biological cells and for their discrimination. From integrated light-scattering measurements, one can already distinguish two subpopulations, T8a and T8b, within T8-positive lymphocytes, which cannot be distinguished by ordinary histological methods.[9]

Retrieval of parameters of a single particle or an ensemble of particles by an angular pattern of scattered light is an important problem of the light-scattering theory.[10–18] To solve that problem (the inverse light-scattering problem), it is nec-

Address all correspondence to Gennady Ruban, Stepanov Institute of Physics, Ave Nezavisimosti 68-Minsk, 220072, Belarus; Tel.: 375 17 2840797; Fax: 375 17 2840879; E-mail: ruban@dragon.bas-net.by

1083-3668/2007/12(4)/044017/11/$25.00 © 2007 SPIE

essary to have optical models of the single scatterer or the ensemble of scatterers. One of the simplest models for single scatterer is the model of homogeneous spherical particle.[17] This simplified model can unlikely be used for the description of light scattered by white blood cells, which we address in this investigation, as they have complex shape and constitution. Models of leukocytes should include a number of parameters,[17–20] in particular, refractive index[21–24] (the relative refractive index for leukocytes is in the range of about 1.01 to 1.08), cell shape size, nuclear shape and size, etc. A model for the ensemble of particles has to include the size distribution functions as well.[25] That is of importance not only within the framework of flow cytometry[26] but also beyond. Some models of biological cells and optical scattering phenomena in whole single cells, as well as in specific cellular organelles isolated from cells or *in situ*, are considered in Refs. 17 and 27–39. The cervical-cell model takes into account intranucleus structure.[36,37]

There are some approaches and techniques that can be used to construct a morphometric model for leucocytes. Different methods are used to obtain data on cell sizes. Among these methods are the centrifugal elutriation technique, tracking velocimetry, light, and electron microscopy,[40] and electronic particle volume analyzing.[41,42]

The technique of centrifugal elutriation for cell size determination is based on a balance between centrifugual sedimentation and centripetal flow.[43,44] By the method of centrifugal elutriation, the authors in Ref. 44 have calculated sizes of some human peripheral blood and bone marrow cells. Tracking velocimetry determines cell size by experimental determining of cell settling velocity in the natural gravity field from microscopically obtained cell images. Human lymphocyte and fibrosarcoma cell size distributions were obtained by the method of tracking velocimetry.[45] The assumptions of the technique are: 1. the cell density does not vary from cell to cell in a given sedimentation subpopulation, and 2. the cells are spherical. Both techniques do not permit obtaining cell parameters (cell and nucleus shapes, nuclei sizes, the location and allignment of a nucleus in the cell, etc.) that significantly influence light-scattering pattern.

Light microscopy enables the size of cells on a smear or in a suspension to be directly measured. Blood smears are very informative for analysis of normal and pathological cells. The data on microscopy-measured leukocytes sizes are basically obtained from blood smears (see Refs. 26, 46, and 47). It is worth noting that cell sizes can be distorted in smears by the smearing and drying effect, as well as by adhesive interaction of cells with a substrate.

Some fine details of cell morphology resolvable with electron microscopy are seemingly redundant for development of a leukocyte model within the framework of scanning flow cytometry today. It is worth noting that electron microscopy methods[40,48] deal with lifeless bio-objects in high vacuum environments.

The Coulter technique[42,49,50] determines cell volume and concentration in suspension. Data from Coulter counters are very useful in many applications.[49] The electronic signal of such counters is not directly related to cell volume.[45] Furthermore, the cell nuclei volumes measured by Coulter counters may be greatly distorted with respect to the data measured by image analysis.[51] Besides, Coulter counters do not determine cell shape parameters that have an influence on light scattering.

Known leukocyte size data are rather conflicting. Discrepancies are seen between cell sizes obtained by examination of smears[47,52] or suspensions,[53] as well as between data of different authors.[47,52]

Although, as we have just described, there are vast data on cell morphology, but a morphometric model for leucocytes with reference to scanning flow cytometry has not been developed yet. The direct light-microscopy investigation of cells in suspension has to be the basis to get more adequate data on cell morphology as applied to the solution of the inverse light-scattering problem for scanning flow cytometry.

As we wrote before, in scanning flow cytometry the importance of a scattering channel is increased, owing to measurement of angular structure of scattered light in a wide range of scattering angles. It brings new opportunities for cell discrimination and potentially can decrease the amount of fluorochrome-labeled (monoclonal) antibodies at the cell analysis. To discriminate the cell we have to correlate its structure and angular pattern. Remember that high rate analysis is very essential to scanning flow cytometry. The recorded angular patterns have to be analyzed rapidly in a real-time scale (typically on the order of miliseconds). That is why it is important to find ways to improve the computer simulation. To solve this problem, we have to narrow domains of uncertainty of morphometric parameters of the cells in question, as applied to the specified scanning flow cytometry technique.

The goal of the work is the optical microscopy investigation of morphometric characteristics of human granulocytes and lymphocytes, at conditions corresponding to that of scanning flow cytometry dealing with high rate analysis of the cells in suspension. On the basis of the data gained by optical microscopy, dot estimations of the distribution parameters of granulocytes, lymphocytes, and nuclei sizes of the cells are obtained. Probability density functions of granulocytes and granulocyte lobes, and lymphocyte and lymphocyte nuclei are estimated. The interrelations between the cell and nucleus metric characteristics for granulocytes and lymphocytes are deduced. The main attention is concentrated on granulocytes. More detailed data on lymphocytes are published by us in another work.[54] The obtained results are used to construct the models of normal cells. The next step is the investigation of pathologic cells.

There are four sections in the work. Section 1 is the introduction, where the general problem is presented. It includes our summary on the known cell morphology data and on their applicability for morphometric model elaboration with reference to scanning flow cytometry. Section 2 is material and methods. The object and method of our investigation are considered. Section 3 is the lymphocyte and granulocyte structure: results and discussion. Here the results of our measurements for granulocytes and lymphocytes by use of optical microscopy are described. We analized the known electron-microscopy data with reference to the scanning flow cytometry and incorporated them into the granulocyte model. The proper references to the original publications of electron-microscopy data are made. Section 4 has the conclusions. Here some remarks on the obtained results are made.

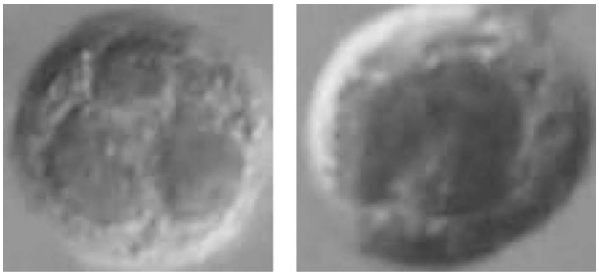

Fig. 1 Images of (a) segmented (neutrophilic) granulocyte and (b) stab (neutrophilic) granulocyte with C-like nucleus shape. Differential interference contrast mode.

2 Materials and Methods

Cells of fresh peripheral blood were investigated. The blood was obtained by venipuncture from apparently healthy men and women ages 20 to 46. Heparin (20 units per 1 ml of blood) was utilized as an anticoagulating agent. The blood was diluted in physiologic saline (pH=7.4) at a ratio of two to one.

Leukocytes were isolated by a density gradient technique. To obtain mononuclear cells (MNCs) or granulocytes in accordance with the last technique, 3 ml of Ficoll-Verografin (Sigma, St. Louis, Missouri) was placed in a tube. Ficoll-Verografin density was 1.097 and 1.077 g/cm^3 for granulocyte and lymphocyte separation, respectively. The blood (4 to 5 ml) was layered over the Ficoll-Verografin cushion. The tube was centrifuged at 460 g at +5 °C for 60 to 80 min. During centrifugation, the cells are separated at phase interface, according to their density.

The isolated fractions of the cells were resuspended in a phosphate buffered (physiological) saline (PBS, pH 7.4) supplemented with 1% heat inactivated pooled AB(IV) serum from five healthy individuals. The resuspended cells were pelleted by centrifugation at 460 g at +5 °C for 20 min. The cell pellets were then washed twice by resuspending in phosphate buffered saline (PBS) with the AB(IV) serum and centrifugation at 210 g at +5 °C for 10 min.

Viability of the isolated cells was determined by a standard technique with the help of trypan blue stain (Sigma, USA). The viability of isolated MNCs and granulocytes being tested with 500 to 600 cells for each individual was ranged from 95 to 100%. The viable and fixed cells were studied. The cells were fixed with 2% solution of paraformaldehyde (Sigma, USA) in PBS at +4 °C in the dark for 20 min, washed in the PBS.

Light microscopy was used to investigation the cell suspensions. For that purpose they were hermetically sandwiched between an object-plate and cover-slip, which makes up a "microcuvette." We used the Leica DMLB2 microscope in the bright field, fluorescence, and differential interference contrast (DIC) modes as per the microscope manufacturer's instructions. An oil immersion objective was used with magnification 100× and numerical aperture 1.25. Optical micrographs were made by the microscope-mounted digital camera Leica DC 150 with a resolution of ~5 MPixels. The granulocyte micrographs in Fig. 1 are displayed as an example. The Leica image processing software IM 1000 has been exploited to analyze 2-D images of the cells. Size calibration was made with a Leica test object.

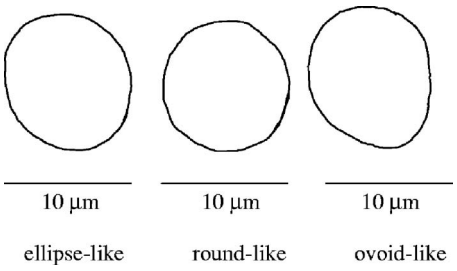

Fig. 2 Contours of granulocytes.

The mononuclear suspensions included lymphocytes and monocytes. We recognized and excluded monocytes via microscopically visual differences in cell morphology. We distinguished B lymphocytes from the mononuclear cells by the fluorescently labeled (with phycoerythrin) monoclonal antibodies directed against surface antigen CD19.

3 Granulocyte and Lymphocyte Structure: Results and Discussion

In this section we consider lymphocyte and granulocyte shapes and sizes and estimate size distribution laws for granulocytes, their lobes, lymphocytes, and their nuclei. Correlations between cell and nucleus metric characteristics for granulocytes and lymphocytes are described.

To construct the adequate model, it is desirable to measure cells having the least possible disturbance. So initially, viable cells were studied. However, the process of cell image recording is time consuming. That is why it is preferable to deal with fixed cells. The fixation can change cell morphological characteristics. To estimate the influence of fixation, we compared fixed and viable cells for some individuals. We detected differences of mean sizes of viable and fixed cells for the same individuals. The differences were small. They did not exceed 1% (for lymphocytes) and 3 to 5% (for granulocytes). For example, mean sizes of viable and fixed lymphocytes were 6.65 and 6.70 μm, respectively (individual 4); mean sizes of viable and fixed granulocytes was 9.24 and 9.52 μm, respectively (individual 11). That is why we do not distinguish the results for viable and fixed cells described next.

3.1 *Lymphocyte and Granulocyte Shape*

Some researchers consider lymphocytes as perfect spherical particles, while others consider them as nonspherical particles.[40,55–57] Our image analysis of the cells has shown that lymphocytes and their nuclei basically have an ellipsoidal shape or a shape close to the spherical one. The lymphocyte nucleus commonly has ellipsoidal or round shapes and sometimes more complex ones. Detailed lymphocyte morphometric data are presented in our article.[54]

Some contours of granulocytes, drawn with Leica image management software IM1000, are displayed in Fig. 2. Contours of granulocytes are less various in shape compared to lymphocyte[54] ones. Our measurements and analysis indicate that the shape of granulocytes is commonly slightly elongated

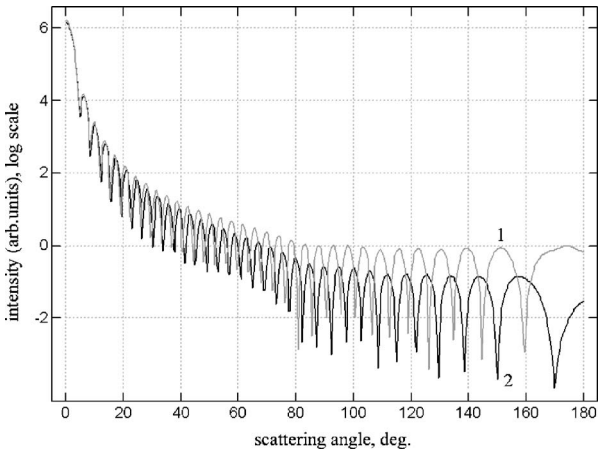

Fig. 3 Calculated angular dependences of light-scattering intensity for the single coated (line 1) and uncoated (line 2) particles with diameter 7.5 μm and refractive index 1.37. Refractive index of particle surroundings is 1.35. Shell thickness of coated particles is 10 nm, and shell refractive index is 1.52. Wavelength of the incident light is 0.63 μm.

(ellipsoidal) or round. Sometimes we observe granulocytes of ovoid-like and other shapes. The mean ratio of the major and minor granulocyte axes (maximum and minimum linear sizes) measured for one of the individuals (individual 6) is 1.08 (standard deviation σ=0.06). This value shows that granulocytes, as well as lymphocytes, are elongated cells. Note that slightly elongated and rounded granulocytes are indicated in the known cell micrographs[40] and figures[46] as well.

According to our estimates, about 90% of granulocyte nuclei are segmented (lobulated). The lobes have different shapes. Sometimes they can be modeled as ellipsoidal-like one. The lobes are more elongated than the granulocyte. For one of the considered individuals, the mean ratio of the major and minor lobe axes is 1.2 (σ=0.1). Nuclei in stab (neutrophilic) granulocytes have C-like, S-like, and other shapes.

Granulocyte surfaces can expose some features.[55] Sometimes we observed a knobby contour of granulocytes by optical microscope. As it was shown by electron microscopy, the surface of neutrophil granulocytes can be wrinkled.[58] Granulocyte nucleus surfaces can also have some features. For example, neutrophil nuclei can be folded.[56]

As it is well known, lymphocytes and granulocytes are surrounded by a plasma membrane with a nanometer-scale thickness. Cell membranes are composed mostly of lipids and proteins with refractive indexes in the range of 1.46 to 1.54 (see Ref. 59 and references therein). Backscattered light calculated for particles with a thin shell is strongly sensitive to shell thickness and to shell refractive index, as one can see from Fig. 3 (our original data are obtained using a code by Babenko, Astafyeva, and Kuzmin[25]) and data published in Ref. 59. Thus the cell membrane should be taken into account in the construction of detailed cell morphometric and optical models, with reference to scanning flow cytometry, when measurement of light intensity scattered in the backward hemisphere is available.

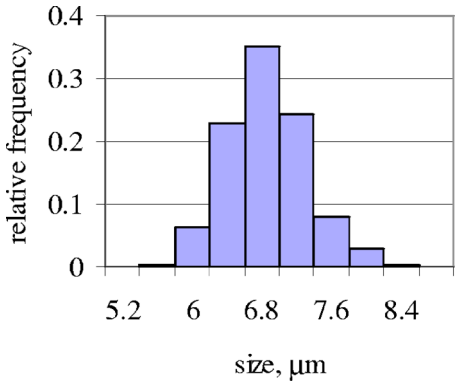

Fig. 4 Histogram of the maximal linear sizes for lymphocytes. Individual 1, n=324.

3.2 *Size Data for Lymphocytes and Granulocytes*

Size of a cell is one of its most important biological and optical parameters. Some results of our measurements for size distributions of lymphocytes and lymphocyte nuclei are shown in Figs. 4 and 5, respectively. Here the maximal linear sizes (major axes) of lymphocytes and lymphocyte nuclei are presented. In Figs. 4 and 5, the relative frequency p_i is plotted on the y axis. The relative frequency $p_i=f_i/n$, where f_i is the observed absolute frequency corresponding to the i'th interval of sizes ($i=1,2\ldots k$, where k is the quantity of the intervals and n is the amount of sampling). Maximum linear size is on the x axis. The range of the sizes, the sampling average size, and the standard deviation for lymphocytes of some individuals are presented in Table 1. These values for lymphocyte nuclei of two individuals are as follows: 4.7 to 8.9, 6.4, and 0.7 μm (individual 1): and 4.8 to 8.3, 6.3, and 0.5 μm (individual 14), respectively. Our measurements demonstrate that a nucleus within a lymphocyte is generally eccentric and off-oriented.[54,60] The lymphocyte nucleus is sometimes situated near the cell membrane. Applying this to the problem of light scattering by the cell results in the appearance of high-order modes in the expansion of the cell internal fields.[18] Comparison of our data on lymphocyte size with data from Coulter counters[45] shows good agreement between the results.

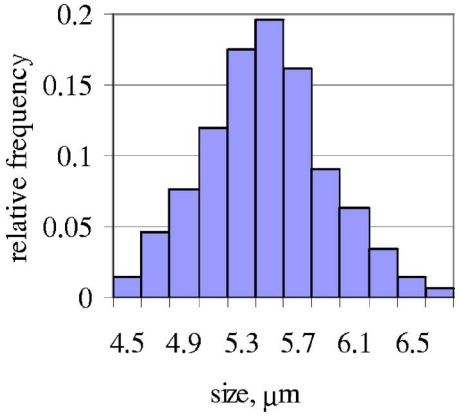

Fig. 5 Histogram of the maximal linear sizes for lymphocyte nuclei. Individual 26, n=474.

Table 1 Lymphocyte size data.

Individual	Range of lymphocyte size, μm	Mean value of lymphocyte size, μm	Standard deviation, μm	Number of cells
2	6.1 to 8.8	7.4	0.5	809
4	5.2 to 8.0	6.6	0.4	324
5	6.3 to 8.6	7.5	0.4	138
23	6.4 to 9.8	7.9	0.6	223
24	6.7 to 9.0	7.7	0.6	168
25	6.3 to 10.1	8.2	0.8	124

In this investigation we mostly pay main attention to granulocytes. The range of sizes, the sampling average size, and the standard deviation for granulocytes are presented in Table 2. The mean size of granulocytes is larger than the one of lymphocytes, as can be seen from Tables 1 and 2. The size ranges of the granulocytes and lymphocytes overlap. Histograms of the granulocyte size (the maximal cell size) distribution as well as the ratio distribution of the maximal and minimal sizes of granulocytes for one individual are presented in Figs. 6 and 7, respectively.

Granulocyte nuclei are frequently lobulated. The nucleus lobes are connected by thin filaments of chromatin.[56] We observed adjoined, overlapped, and separated nucleus lobes. For the individuals that we examined, the number of nuclei lobules in granulocyte set is in the range 2 to 6, commonly 3 to 4. Granulocyte subsets are characterized by other researchers as follows[61]: neutrophil granulocytes contain 3 to 5 lobules, basophils contain 2 to 3 lobes, and eosinophils contain 2 lobes commonly. The range of the maximal linear sizes, the sampling average size, and the standard deviation for single nucleus lobes in our measurements are 2.6 to 6.6, 4.35, and 0.65 μm, respectively. These values for minimal linear size (minor axis) of nucleus lobes are 2.4 to 5.7, 3.6, and 0.55 μm, respectively (individual 9). Total projection area of the granulocyte lobes (of the 2-D cell images) is in the range of 21 to 49 μm^2; the mean total area is 33 μm^2 with standard deviation 5.5 μm^2 (individual 9). Histograms of the measured size distributions of nuclei lobes are displayed in Figs. 8–10.

Table 2 Granulocyte size data.

Individual	Range of granulocyte size, μm	Mean value of granulocyte size, μm	Standard deviation, μm	Number of cells
6	8.0 to 11.7	9.6	0.5	3040
7	7.9 to 12.1	9.7	0.7	583
8	8.1 to 12.0	9.6	0.6	697
9	7.9 to 11.2	9.5	0.6	225
10	7.3 to 12.1	9.4	0.7	187
11	7.6 to 13.2	9.2	0.7	316
12	7.8 to 13.0	9.8	0.9	118
15	7.9 to 12.4	9.4	0.7	326

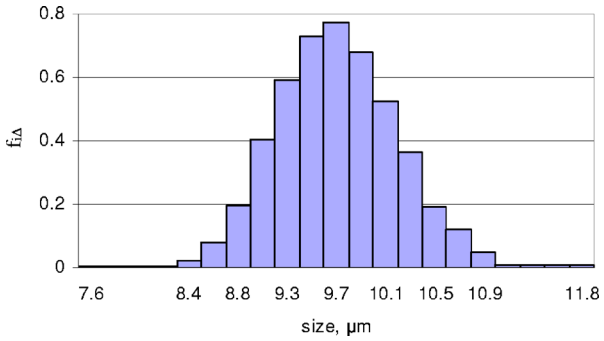

Fig. 6 Histogram of the maximal linear sizes for granulocytes. Individual 6, n=3040.

Compare our data for the ratios of the cell to nucleus size for lymphocytes and granulocytes. The mean ratio of the major axis of lymphocytes to its nucleus axis is about 1.2. This means that in the majority of cells the nucleus and lymphocyte sizes are comparable. We characterize the size of a granulocyte nucleus by its effective diameter. It is determined as the diameter of the disk having the same area as the total area of the granulocyte lobes. Effective diameter of a granulocyte is the diameter of the cell equiarea-disk. The mean ratio for the effective diameters of a granulocyte and the granulocyte lobes is about 1.6.

As it is known, granulocyte cytoplasm holds granules.[61] They have sizes close to the limit of the light microscope resolution. Published data of electron-microscopy studies are contradictory. Electron-microscopy micrographs commonly display elongated granules.[61,62] Analyzing the micrographs of eosinophil granules, as published in Refs. 61 and 62, we find that the ranges of ratios of maximal and minimal sizes are 1.2 to 1.7 and 1.2 to 2.5, respectively. According to the results of Ref. 56, the eosinophil granules have spherical shapes; basophil granules are roughly spherical or are seldomly, irregular.

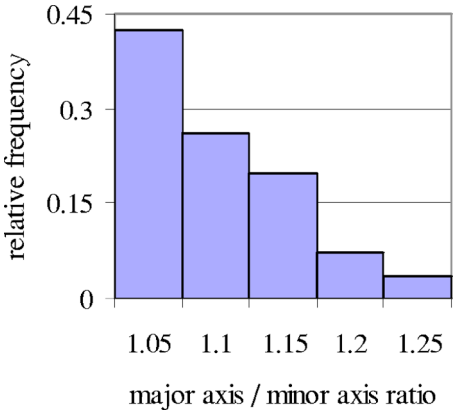

Fig. 7 Ratio distribution of the maximal linear size to the minimal one for granulocytes. Individual 6, n=112.

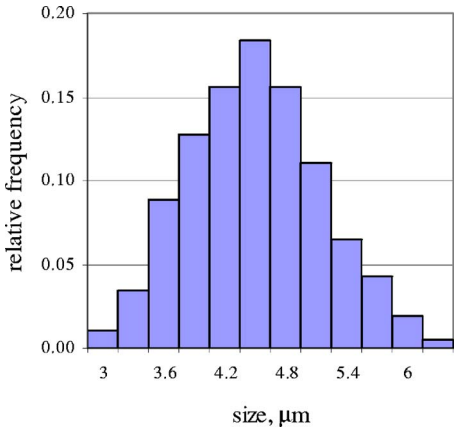

Fig. 8 Histogram of the maximal linear sizes for granulocyte lobes. Individual 9, $n=462$.

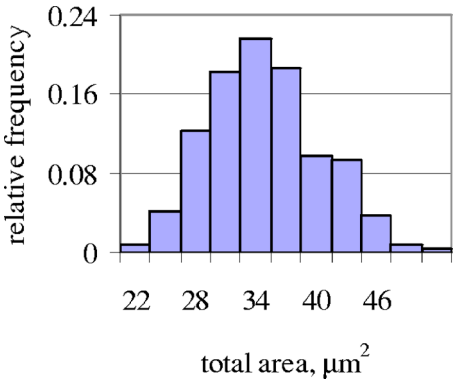

Fig. 10 Total-area distribution of granulocyte lobes cross-sections. Individual 9, $n=236$.

Granules are different in organization. For example, specific eosinophil granules are heterogeneous: they include a peripheral matrix and inner core. This core is an elongated crystalloid.[61,63] Other eosinophil granules are homogeneous (coreless).[56]

Granules in granulocyte subsets are various in size. The neutrophil granulocyte cytoplasm holds specific granules with a size of about 0.2 μm (80 to 90% of the total number of granules) and nonspecific ones with a size of about 0.4 μm (10 to 20%). Basophil granulocytes contain specific granules with sizes 0.5 to 1.2 μm. Sizes of specific granules in eosinophil granulocytes are 0.6 to 1 μm. The previous data are obtained by electron microscopy.[61] The lower limit of specific eosinophil granules measured by the time-resolved patch-dampt capacitance technique is 0.45 to 0.5 μm.[64] The surface area of eosinophil granules is about 0.7 μm^2.[64]

Some comments on granule packing and ordering are as follows. Granules occupy a noticeable part of the cytoplasm, as one can see from electron micrographs.[61] This visual impression is verified by numerical data. For example, the area of granulation in eosinophils is 87%.[26] The number of grains in the cytoplasm of neutrophil granulocytes is 50 to 200. Reciprocal disposition and orientation of elongated granules is not fully random, as seen from the electron micrographs of granulocytes.[61,62]

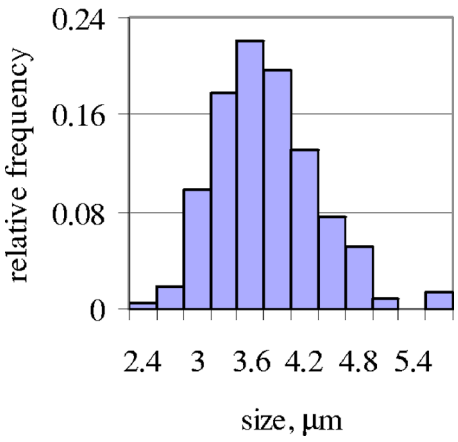

Fig. 9 Histogram of the minimal linear sizes of granulocyte lobes. Individual 9, $n=213$.

We analyze the described electron-microscopy data on granulocyte granules with reference to scanning flow cytometry. First, the previously mentioned high value of area filling of the cytoplasm by granules (0.87) implies that at first approximation, when constructing a model for granulocyte morphology, intracellular constituents other than granules (and nucleus) can be neglected. Second, we deduce that granulocyte granules are an ensemble of densely packed particles in terms of optics of scattering media. Granule disposition and orientation are partially ordered. Dense packing gives rise to overirradiation and near-field effects.[65,66] Ordered disposition and orientation give rise to interference of light scattered by granules. These facts should be taken into account when selecting a proper method to solve direct and inverse light-scattering problems. Third, the size of granulocyte granules is less than or comparable with the wavelength of visible light. Such particles have a larger ratio of sideways and backward light-scattering intensity compared to particles larger than a wavelength. Therefore, angular light-scattering patterns by a granulocyte should have distinctive features as compared to an agranulocyte of a proper size, e.g., a monocyte and a large lymphocyte. Fourth, the size of the majority of neutrophil granulocyte granules is approximately 3 to 6 times smaller than that of eosinophil and basophil granulocytes. Thereafter, the angular scattering pattern of light by neutrophil granulocytes can expose distinctive features as compared with the one for eosinophil and basophil granulocytes. Fifth, having analyzed the previously listed data, it is reasonable to conclude that distinctive polarization features of scattered light correspond to the elongated and partially ordered eosinophil granules with crystalloid cores. These features can be used to distinguish eosinophils.

A major subset of granulocytes is neutrophils. The morphometric model of a neutrophilic granulocyte with lobulated nucleus is shown schematically in Fig. 11.

Some comparisons of our results with the data of Coulter measurements and smear measurements for the size of granulocytes are indicated next. The average neutrophilic granulocyte volume as measured with a Coulter counter is 370 fL.[53] The corresponding neutrophil diameter is then 8.9 μm for an

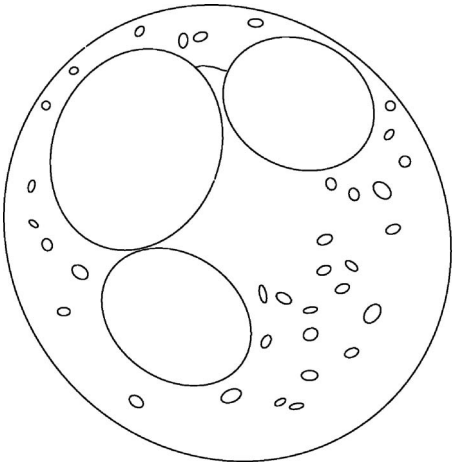

Fig. 11 Scheme of lobulated neutrophil granulocyte.

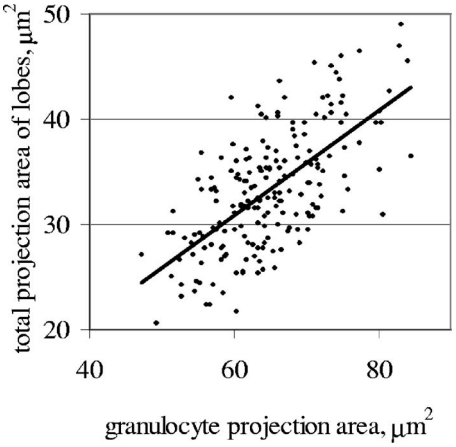

Fig. 12 Scatter plot (points) and linear regression (solid line) of the projection area of granulocytes and total projection area of the granulocyte lobes. Individual 9, $n=193$.

equivolume sphere. The mean size of 9.58 μm of granulocytes, as we observed, is slightly larger inasmuch as the granulocytes in our measurements include neutrophils, eosinophils, and basophils. The last two are larger in size than neutrophils.[52] Moreover, a granulocyte actually is a somewhat oblong ellipsoid rather than a perfect sphere. So our size data agree well with the literature data for lymphocytes and granulocytes in suspension. We measured size ranges of granulocytes in suspension. The lower and upper limits of the ranges for different individuals are 7.3 and 13.2 μm, respectively. It worthwhile to note that the sizes of granulocytes in a smear (12 to 17 μm)[47,52] and in suspension (7.3 to 13.2 μm) are noticeably different. The lower limit (12 μm) of the granulocyte-size ranges in a smear is close to the upper limit of the ranges in suspension (13.2 μm).

Our measurements and calculations have shown that there is a positive correlation between areas of granulocyte lobes and of the granulocyte itself. It is statistically highly significant, the probability $P<0.0001$. The probability P is determined as follows: $P=P_N(|r|\geq r_0)$, where r is the correlation coefficient, and r_0 is the sampling correlation coefficient.[67] Values of correlation coefficients for two individuals are indicated in Table 3. Constants A_g and B_g of the linear regression equation $(y=A_g+B_gx)$ of the lobe area y on granulocyte area x are presented in Table 3 as well. The experimental data of the lobes and granulocyte areas are displayed in Fig. 12. A linear correlation dependence of sizes for T-lymphocyte and its nucleus[54] and B-lymphocyte and its nucleus (Table 4) are also revealed. Constants A and B of the linear regression equation $(y=A+Bx)$ of nucleus size (major nucleus axis y) on lymphocyte size (major lymphocyte axis x) for B-cells are presented in Table 4. Correlation coefficients between sizes of nucleus and B-lymphocyte for some individuals are indicated in the table as well.

The discovered correlations of metric characteristics for the cells and their nuclei simplify simulations of scattering patterns. Actually, the correlations reduce a *set* of cell-nucleus size combinations to the statistically admissible *subset* of the combinations. Just this subset has to be taken into consideration under simulation of cell scattering patterns. It permits faster analysis of light scattering to discriminate cells in a real-time scale.

3.3 *Estimation of a Size Distribution Law*

In this subitem, the distribution density of granulocytes and lymphocytes is estimated. To promote a hypothesis for distribution law $f(x)$ of the cell sizes, we 1. calculate the dot evaluation of distribution parameters of granulocytes, and 2. construct a histogram of size distribution of these cells. Then 3. we check the hypothesis by an evaluation of the probability density function in accordance with criterion χ^2.

3.3.1 *Estimation by Dot Parameters*

For an initial assessment of the distribution law, it is expedient to use a simple method. To make a conclusion about the distribution law, the scheme of sampling dot evaluations obtained by a method of moments is used.[67] According to this

Table 3 Sampling correlation coefficient and constants A_g and B_g of the linear regression equation of granulocyte lobe area on granulocyte area.

Individual	Correlation coefficient	A_g, μm^2	Standard deviation of A_g, μm^2	B_g	Standard deviation of B_g	Standard deviation of lobe area, μm^2	Number of cells
9	0.65	1	0.2	0.5	0.04	4.3	193
16	0.41	6.3	0.3	0.25	0.03	3.5	285

Table 4 Constants A and B of the linear regression equation of nucleus size on lymphocyte size for B-cells.

Individual	A, μm	Standard deviation of A, μm	B	Standard deviation of B	Standard deviation of nucleus size, μm	Correlation coefficient between nucleus and lymphocyte sizes
30	1.9	0.06	0.5	0.15	0.6	0.61
31	2.7	0.75	0.5	0.1	0.5	0.62
32	3.6	0.7	0.4	0.1	0.4	0.55

scheme, the sampling values are calculated for the factors of asymmetry A and excess E, and their standard deviations S_A and S_E.

Then it is believed that the empirical law is consistent with the hypothetical one, provided that the following inequalities hold:

$$|A - M(A)| < 3S_A, \tag{1}$$

$$|E - M(E)| < 3S_E, \tag{2}$$

where $M(A)$ and $M(E)$ are the mathematical expectations of the A and E values.

As a hypothesis, let us consider the normal law of distribution of the experimental data. For the normal distribution we have: $M(A)=M(E)=0$. Calculation of the values A, E, S_A, and S_E shows that inequalities in Eqs. (1) and (2) are carried out for the individuals. Hence, the hypothesis about normal distribution is accepted. It is worth noting that the inequalities in Eqs. (1) and (2) have empirical basis, and the obtained conclusion has to be considered as the preliminary one. Further analysis is carried out next.

3.3.2 *Estimation by Histogram*

For construction of the histogram, the range of the measured values of cell sizes is divided into the intervals of width Δ_i. Then the absolute frequency f_i, the relative frequency $p_i = f_i/n$, and the normalized relative frequency $f_{i\Delta}=f_i/(n\Delta_i)$, corresponding to the intervals, are counted up (n is the amount of sampling). On the basis of that data, the histogram of granulocyte size distribution is constructed (Fig. 6).

The obtained sampling estimations of the distribution parameters and the constructed histogram allow putting forward a hypothesis H_0 of the normal distribution law. A detailed check of that hypothesis is carried out in the following.

3.3.3 *Estimation by the Chi-square Criterion*

To test the identity of the distribution density of the sample data, and the hypothetical distribution density, the χ^2 criterion is used by the following scheme.[67]

1. A hypothesis $H_0 f(x)=f_0(x,\theta)$ is put forward. Here $f(x)$ is a distribution law of the random value represented by the sample $\{x_j\}$, $j=1\ldots n$. $f_0(x,\theta)$ is the model distribution law characterized by a vector of parameters $\theta=[\theta_1\ldots\theta_m]$.

2. The range of the measured sizes is divided into k grouping intervals of width Δ_i with X_i as the right boundary of an i'th interval, $i=1\ldots k$. Absolute frequency f_i appropriate to the i'th interval is counted up over the sample $\{x_j\}$. Some intervals on the tail areas of the distribution are combined to provide for statistical representativeness of frequency f_i (in that case $i=1\ldots k_0$, $k_0<k$), and an expected probability $P_i = \Phi(Z_{i+1})-\Phi(Z_i)$ is calculated. Here the function

$$\Phi(Z) = \int_{-\infty}^{z} \exp(-t^2)dt, \tag{3}$$

is the distribution function of the standardized normal random value Z with zero mean $Z_m=0$ and unit variance $\sigma_z^2=1$. The expected absolute frequency $F_i=P_i n$ $(i=1\ldots k_0)$.

3. Checking on the hypothesis includes three steps.

Step 1. A critical point $\chi^2_{\alpha\nu}$ is determined for a significance level α and the degrees of freedom $\nu=k_0-1-m$. Under a statistical treatment of the results of medical investigations, it is often agreed that $\alpha=0.01$. The values of $\chi^2_{\alpha\nu}$ are tabulated (see Ref. 67).

Step 2. A value of criterion χ^2 is calculated.

$$\chi^2 = \sum_i^{k_0} \chi_i^2 = \sum_i^{k_0} (F_i - f_i)^2/F_i. \tag{4}$$

Calculation of the χ^2-criterion value is elaborated for one individual in Table 5.

Step 3. Comparing the criterion χ^2 value with the $\chi^2_{\alpha\nu}$ value, we accept or reject the hypothesis H_0 on the significance level α. The domain of acceptance of the hypothesis is determined by an inequality $\chi^2 \leq \chi^2_{\alpha\nu}$.

The considered scheme is used to analyze measurement results. The previous inequality is fulfilled for all considered individuals. For example, for individual 6, the value of $\chi^2 = 23.34$ (for granulocytes). It is less than the value of the critical point for this individual ($\chi^2_{\alpha\nu}=26.21$). Hence, on the significance level $\alpha=0.01$, we do not have ground to reject hypothesis H_0 of the normal distribution law

$$f(x) = 1/[(2\pi)^{1/2}\sigma]\exp - (x - x_m)^2/2\sigma^2. \tag{5}$$

For the experimental data grouped in Table 5 (individual 6), $x_m=9.58$ μm, and $\sigma=0.52$ μm.

The values of criterion χ^2 are close to the proper critical points $\chi^2_{\alpha\nu}$ for the considered individuals. That is why it is reasonable to examine other distribution laws. Assuming normal distribution of logarithms of the measured values, we

Table 5 The data to calculate the χ^2criterion and to test the hypothesis of normal granulocyte size distribution (individual 6).

i	X_i	fi	Z_i	$\Phi(Z_i)$	P_i	F_i	χ_i^2
1	8.20	12	−2.6545	0.0040	0.0040	12.0735	0.0004
2	8.41	13	−2.2495	0.0122	0.0083	25.1398	5.8622
3	8.62	52	−1.8445	0.0326	0.0203	61.7630	1.5433
4	8.83	124	−1.4394	0.0750	0.0425	129.0594	0.1983
5	9.04	257	−1.0344	0.1505	0.0755	229.3805	3.3256
6	9.25	376	−0.6294	0.2645	0.1141	346.7701	2.4638
7	9.46	465	−0.2244	0.4112	0.1467	445.9143	0.8169
8	9.67	493	0.1806	0.5717	0.1604	487.7392	0.0567
9	9.88	433	0.5856	0.7209	0.1493	453.7889	0.9524
10	10.09	334	0.9906	0.8391	0.1181	359.1265	1.7580
11	10.30	233	1.3956	0.9186	0.0795	241.7494	0.3167
12	10.51	122	1.8006	0.9641	0.0455	138.4213	1.9481
13	10.72	76	2.2057	0.9863	0.0222	67.4136	1.0936
14	10.93	30	2.6107	0.9955	0.0092	27.9246	0.1542
15	11.14	20	3.0157	0.9987	0.0045	13.7358	2.8568

found that χ^2 values are noticeably smaller than the proper $\chi^2_{\alpha\nu}$ values (for example, for individual 6, criterion $\chi^2 = 11.11$) It means that the log-normal law

$$f(x) = 1/[(2\pi)^{1/2} x\sigma]\exp(-[\ln(x/x_m)]^2/2\sigma^2), \qquad (6)$$

describes the experimental data better than the normal one. Parameters x_m and σ of the log-normal distribution law for granulocytes, granulocyte lobes, lymphocytes, and lymphocyte nuclei are displayed in Table 6 for some individuals.

The graphics of normal and log-normal distributions and experimental data are displayed in Fig. 13 for one individual. The experimental data are taken from the histogram of Fig. 6. Figure 13 shows that both distributions agree well with the experimental data and the log-normal law describes the measurement results better.

4 Conclusions

The peripheral blood granulocytes and lymphocytes of healthy adult individuals are investigated by methods of specialized light microscopy. The morphometric parameters of the cells in suspension are measured and analyzed. The cell structures are characterized as applied to a problem of cell discrimination in the frame of polarizing scanning flow cytometry.

Size distribution parameters of the cells and nuclei are statistically estimated. The size probability density functions of cells and their nuclei are obtained on the base of the estimated parameters. The interrelations between the cell and nucleus

Table 6 Parameters x_m and σ of log-normal size distribution calculated by criteria χ^2 for granulocytes, granulocyte lobes, lymphocytes, and lymphocyte nuclei.

Individual	Cell	x_m, μm	σ	Number of cells
6	Granulocyte	9.56	0.054	3040
7	Granulocyte	9.70	0.067	583
8	Granulocyte	9.63	0.063	697
9	Granulocyte lobes	4.31	0.15	462
1	Lymphocyte	7.78	0.056	406
2	Lymphocyte	7.40	0.065	809
14	Lymphocyte	7.67	0.079	1089
14	Lymphocyte nuclei	6.30	0.077	1089

metric characteristics are deduced for granulocytes and lymphocytes to provide the simplification of the computer simulation and the reduction of the running time of cell discrimination algorithms. The obtained data are processed and generalized to construct the morphometric models of a segmented neutrophilic granulocyte and a lymphocyte. Our morphometric data meet the requirements of flow cytometry dealing with the cells in suspension and real-time computations. The findings of our investigation can be used as input parameters to solve the direct and inverse light-scattering problems in scanning flow cytometry, dispensing with costly and time-consuming cell labeling by monoclonal antibodies and fluorochromes, as well as in turbidimetry and nephelometry.

The obtained results are related to cells of healthy individuals. Consideration of pathologic cells is the next step of the investigation. The cell models developed in the present work can contribute to theoretical grounding of cell discrimination and diagnosis methods. These models make it possible to establish relationships between the cell structure and the angular pattern of scattered light to determine dominant and secondary origins of light scattering by a cell. This can provide background for better biological and medical interpreta-

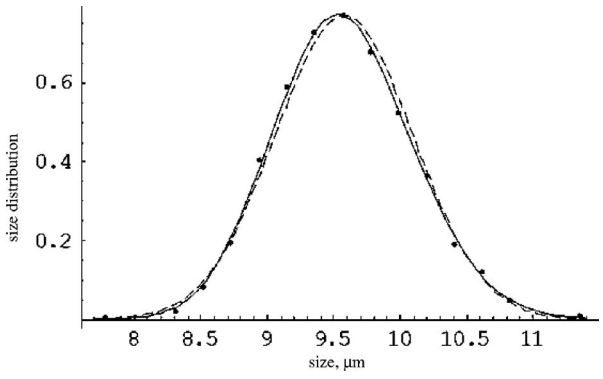

Fig. 13 The granulocyte size distribution $f(x)$. The dashed line is the normal distribution and the solid line is the log-normal distribution. Points $f_{i\Delta}$ indicate experimental data. Individual 6, $n=3040$.

tions of the scattering patterns, to improve discriminating and diagnostic capabilities of immunophenotyping-free scanning flow cytometry, as well as for further adaptation of cell models to the real-time computations.

Acknowledgments

This research was supported by the Programme of Basic Research of Belarus "Modern technologies in medicine", and partially sponsored by NATO's Scientific Affairs Division in the framework of the Science for Peace Programme, Project 977976. We express our gratitude to Olga Gritsai for taking part in the cell image recordings. The authors are thankful to Alfons Hoekstra, Alexei Gruzdev, and Valeri Maltsev for fruitful discussions.

References

1. *Flow Cytometry and Sorting*, 2nd ed., M. R. Melamed, T. Lindmo, and M. L. Mendelsohn, Eds., Wiley-Liss, New York (1990).
2. H. M. Shapiro, *Practical Flow Cytometry* 4th ed., Wiley Liss, New York (2003).
3. V. P. Zharov, E. I. Galanzha, E. V. Shashkov, N. G. Khlebtsov, and V. V. Tuchin, "*In vivo* photoacoustic flow cytometry for monitoring of circulating single cancer cells and contrast agents," *Opt. Lett.* **31**, 3623–3625 (2006).
4. S. Sincock and J. Robinson, "Flow cytometric analysis of microorganisms," *Methods Cell Biol.* **64**, 511–537 (2001).
5. J. L. Castagner and I. J. Bigio, "Particle sizing with a fast polar nephelometer," *Appl. Opt.* **46**, 527–532 (2007).
6. K. Singh, X. Su, C. Liu, C. Capjack, W. Rozmus, and C. J. Backhouse, "A miniaturized wide angle 2D cytometer," *Cytometry* **69A**, 307–315 (2006).
7. V. Maltsev, "Scanning flow cytometry for individual particle analysis," *Rev. Sci. Instrum.* **71**, 243–255 (2000).
8. J. Neukammer, C. Gohlke, A. Hope, T. Wessel, and H. Rinneberg, "Angular distribution of light scattered by single biological cells and oriented particle agglomerates," *Appl. Opt.* **42**, 6388–6397 (2003).
9. L. Testappen, B. de Grooth, G. Nolten, C. Napel, W. van Berkel, and J. Greve, "Physical discrimination between human T-lymphocyte subpopulations by means of light scattering, revealing two populations of T8-positive cells," *Cytometry* **7**, 178–183 (1986).
10. Z. Ulanovsky, Z. Wang, P. Kaye, and I. Ludlov, "Application of neural networks to the inverse light scattering problem for spheres," *Appl. Opt.* **37**, 4027–4033 (1998).
11. P. M. Pilarski and C. J. Backhouse, "A method for cytometric image parameterization," *Opt. Express* **14**, 12720–12743 (2006).
12. K. Semyanov, P. Tarasov, A. Zharinov, A. Chernyshev, A. Hoekstra, and V. Maltsev, "Single particle sizing from light scattering by spectral decomposition," *Appl. Opt.* **43**, 5110–5115 (2004).
13. V. Berdnik and V. Loiko, "Particle sizing by multiangle light-scattering data using the high-order neural networks," *J. Quant. Spectrosc. Radiat. Transf.* **100**, 55–63 (2006).
14. V. Berdnik, R. Mukhamedyarov, and V. Loiko, "Characterization of optically soft spheroidal particle by multiangle light-scattering data by use of the neural-networks method," *Opt. Lett.* **29**, 1019–1021 (2004).
15. A. Doicu, T. Wriedt, and Y. A. Eremin, *Light Scattering by Systems of Particles*, Springer-Verlag, Berlin (2006).
16. M. I. Mishchenko, L. D. Travis, and A. A. Lacis, *Scattering, Absorption, and Emission of Light by Small Particles*, Cambridge University Press, Cambridge, MA (2002).
17. V. P. Maltsev and K. A. Semyanov, *Characterisation of Bio-Particles from Light Scattering*, Brill Academic Publishers, Boston, MA (2004).
18. *Optics of Biological Particles*, A. Hoekstra, V. Maltsev, and G. Videen, Eds., *Nato Science Series, II, Mathematics, Physics, and Chemistry, II/238*, Springer, Dordrecht (2007).
19. F. Bolin, L. Preuss, R. Taylor, and R. Ference, "Refractive index of some mammalian tissues using a fiber optic cladding method," *Appl. Opt.* **28**, 5269–5277 (1989).
20. F. Charriere, A. Marian, F. Montfort, J. Kuehn, and T. Colomb, "Cell refractive index tomography by digital holographic microscopy," *Opt. Lett.* **31**, 178–180 (2006).
21. F. A. Duck, *Physical Properties of Tissue: a Comprehensive Reference Book*, Academic Press, San Diego, CA (1990).
22. K. W. Keohan and W. K. Metcaff, "The cytoplasmic refractive index of lymphocytes, its significance and its changes during active immunization," *Q. J. Exp. Physiol. Cogn Med. Sci.* **44**, 343–346 (1959).
23. J. M. Schmitt and G. Kumar, "Turbulent nature of refractive index variations in biological tissue," *Opt. Lett.* **21**, 1310–1312 (1996).
24. J. J. J. Dirckx, L. C. Kuypers, and W. F. Decraemer, "Refractive index of tissue measured with confocal microscopy," *J. Biomed. Opt.* **10**(4), 1–8 (2005).
25. V. A. Babenko, L. G. Astafyeva, and V. N. Kuzmin, *Electromagnetic Scattering in Disperse Media: Inhomogeneous and Anisotropic Particles*, Springer-Praxis, Berlin (2003).
26. C. Pronk-Admiraal, F. van Haaster, and P. Bartels, "Clinical evaluation of changes in the morphology of eosinophils," *Clin. Chem. Lab. Med.* **40**, 27–31 (2002).
27. B. V. Bronk, S. D. Druger, J. Czege, and W. P. Van De Merwe, "Measuring diameters of rod-shaped bacteria in vivo with polarized light scattering," *Biophys. J.* **69**, 1170–1177 (1995).
28. A. N. Shvalov, J. T. Soini, I. V. Surovtsev, and G. V. Kochneva, "Individual *Escherichia coli* cells studied from light scattering with the scanning flow cytometer," *Cytometry* **41**, 41–45 (2000).
29. A. G. Hoekstra, M. D. Grimnic, and P. M. A. Sloot, "Large scale simulations of elastic light scattering by a fast discrete dipole approximation," *Int. J. Mod. Phys. C* **9**, 87–102 (1998).
30. G. Videen, D. R. Prabhu, M. Davies, F. Gonzales, and F. Moreno, "Light scattering fluctuations of a soft spherical particle containing an inclusion," *Appl. Opt.* **40**, 4054–4057 (2001).
31. A. N. Shvalov, J. T. Soini, A. V. Chernyshev, P. A. Tarasov, E. Soini, and V. P. Maltsev, "Light scattering properties of individual erythrocytes," *Appl. Opt.* **38**, 230–235 (1999).
32. R. Drezec, A. Dunn, and R. Richards-Kortum, "A pulsed finite-difference time-domane (FDTD) method for calculating light scattering from biological cells over broad wavelength ranges," *Opt. Express* **6**, 147–157 (2000).
33. N. N. Boustany, R. Drezek, and N. V. Thakor, "Calcium-induced alterations in mitochondrial morphology quantified in situ with optical scatter imaging," *Biophys. J.* **83**, 1691–1700 (2002).
34. P. L. Gourley, J. K. Hendricks, A. E. McDonald, R. G. Copeland, K. E. Barrett, C. R. Gourley, and R. K. Naviaux, "Ultrafast nanolaser flow device fordetecting cancer in single cells," *Biomed. Microdevices* **7**, 331–339 (2005).
35. P. L. Gourley, J. K. Hendricks, A. E. McDonald, R. G. Copeland, K. E. Barrett, C. R. Gourley, K. K. Singh, and R. K. Naviaux, "Mitochondrial correlation microscopy and nanolaser spectroscopy—new tools for biophotonic detection of cancer in single cells," *Technol. Cancer Res. Treat.* **4**, 585–592 (2005).
36. R. Drezek, M. Guillaud, T. Collier, I. Boiko, A. Malpica, C. Macaulay, M. Follen, and R. Richards-Kortum, "Light scattering from cervical cells throughout neoplastic progression: influence of nuclear morphology DNA content and chromatin texture," *J. Biomed. Opt.* **8**(1), 7–16 (2003).
37. D. Arifler, M. Guillaud, A. Carraro, A. Malpica, M. Follen, and R. Richards-Kortum, "Light scattering from normal and dysplastic cervical cells at different epithelial depths: finite-differences time domain modeling with a perfectly matched layer boundary condition," *J. Biomed. Opt.* **8**(3), 484–494 (2003).
38. R. S. Brock, X.-H. Hu, D. A. Weidner, J. R. Mourant, and J. Q. Lu, "Effect of detailed cell structure on light scattering distribution: FDTD study of a B-cell with 3D structure constructed from confocal images," *J. Quant. Spectrosc. Radiat. Transf.* **102**, 25–36 (2006).
39. J. Q. Lu, P. Yang, and X. Hu, "Simulations of light scattering from a biconcave red blood cell using the finite-difference time-domain method," *J. Biomed. Opt.* **10**(2), 024022 (2005).
40. *Atlas of Scanning Electron Microscopy of Cells, Tissue and Organs*, O. V. Volkova, Ed., Meditsina, Moscow (1982) (in Russian).
41. G. Segel, G. Cokelet, and M. Lichtman, "The measurement of lymphocyte volume: importance of reference particle deformability and counting solution tonicity," *Blood* **57**, 894–899 (1981).
42. H. Alexander, G. Markey, R. Nolan, and T. Morris, "Cell sizing in chronic lymphoproliferative disorders: an aid to differential diagnosis," *J. Clin. Pathol.* **45**, 875–879 (1992).
43. I. Bertoncello, "A comparison of cell separations obtained with centrifugal elutriation and sedimentation at unit gravity, in *Cell Separa-*

tion Methods and Selected Applications, T. G. Pretlow and T. Pretlow, Eds., pp. 89–108, Academic Press, San Diego, CA (1987).
44. L. Lasky and E. Zanjani, "Size and density characterization of human committed and multipotent hematopoietic progenitors," *Exp. Hematol.* **13**, 680–684 (1985).
45. J. Chalmers, S. Haam, Y. Zhao, K. McCloskey, L. Moore, M. Zborowski, and S. Williams, "Quantification of cellular properties from external fields and resulting induced velocity: cellular hydrodynamic diameter," *Biotechnol. Bioeng.* **64**, 509–518 (1999).
46. *Atlas of Blood Morphology in Health and Disease*, Public Health Service, U.S. Department of Health and Human Services, Atlanta, GA (1987).
47. "Atlas of Microscopic Anatomy," see http://www.vh.org/adult/provider/anatomy/MicroscopicAnatomy/Section04/Section04.html.
48. A. Dvorak, S. Ackerman, and P. Weller, "Subcellular morphology and biochemistry of eosinophils," *Blood Cell Biochem.* **2**, 237–344 (1991).
49. E. Chapman, A. Kurec, and F. Davey, "Cell volumes of normal and malignant mononuclear cells," *J. Clin. Pathol.* **34**, 1083–1090 (1981).
50. Coulter® AC·T Series Analyzer, T Series Documentation, Coulter Corporation, Miami, FL 33196 (1997).
51. J. Mourant, M. Canpolat, C. Brocker, O. Esponda-Ramos, T. Johnson, A. Matanock, K. Stetter, and J. Freyer, "Light scattering from cells: the contribution of the nucleus and the effects of proliferative status," *J. Biomed. Opt.* **5**(2), 131–137 (2000).
52. "Blood histology. formed elements of the blood," see http://faculty.ucc.edu/biology-potter/blood-histology.htm, and http://www.vh.org/adult/provider/anatomy/MicroscopicAnatomy/Section04/Section04.html.
53. B. Sandro, O. Rotstein, J. J Parodo, M. Phillips, and A. Kapus, "Hypertonic inhibition of exocytosis in neutrophils: central role for osmotic actin skeleton remodeling," *Am. J. Physiol.: Cell Physiol.*, **279**, 619–C633 (2000).
54. V. A. Loiko, G. I. Ruban, O. A. Gritsai, A. D. Gruzdev, S. M. Kosmacheva, N. V. Goncharova, and A. A. Miskevich, "Morphometric model of lymphocyte as applied to scanning flow cytometry," *J. Quant. Spectrosc. Radiat. Transf.* **102**, 73–84 (2006).
55. G. I. Kozinets, V. M. Pogorelov, D. A. Shmarov, S. F. Boev, and V. V. Sazonov, *Blood Cells: Modern Technology of Analysis*, Triada-Pharm, Moscow (2002) (in Russian).
56. Glossary of terms for hematology, see http://www.courses.ahc.umn.edu/medical-school/LaMP/5104/atlas/glossary.html.
57. see http://155.58.145.40/WBC/cells.htm.
58. J. Derganc, B. Bozhich, S. Svetina, and B. Zheksh, "Stability analysis of micropipette aspiration of neutrophils," *Biophys. J.* **79**, 153–162 (2000).
59. R. A. Meyer, "Light scattering from biological cells: dependence of backscatter radiation on membrane thickness and refractive index," *Appl. Opt.* **18**, 585–588 (1979).
60. V. A. Loiko, G. I. Ruban, O. A. Gritsai, A. A. Miskevich, S. M. Kosmacheva, and N. V. Goncharova, "Investigation of human white blood cells: application to scanning flow cytometry," *Proc. SPIE* **6284**, 6284OH (2005).
61. *Histology, Cytology, and Embryology*, J. A. Afanasjev and N. A. Jurina, Eds., Meditsina, Moskow (2001) (in Russian).
62. D. Zucker-Franclin, M. F. Greaves, C. E. Grossi, and A. M. Marmont, *Atlas of Blood Cells: Function and Pathology*, Vol. **2**, Lea and Febiger, Philadelphia, PA (1988).
63. I. Roitt, J. Brostoff, and D. Male, *Immunology*, Mosby, London (1998).
64. J. Hartmann, S. Scepec, and M. Lindau, "Regulation of granule size in human and horse eosinophils by number of fusion events among unit granules," *J. Physiol. (London)* **483**, 201–209 (1995).
65. A. P. Ivanov, V. A. Loiko, and V. P. Dick, *Light Propagation in Densely Packed Media*, Nauka i Technika, Minsk, Belarus (1988) (in Russian).
66. V. A. Loiko and G. I. Ruban, "Absorption by a layer of densely packed subwavelength-sized particles," *J. Quant. Spectrosc. Radiat. Transf.* **89**, 271–278 (2004).
67. J. Bendat and A. Piersol, *Random Data: Analysis and Measurement Procedures*, John Wiley and Sons, New York (1986).